ADVANCED MATERIALS

slightly changed after their incorporation in polymer matrices, the optical properties of the resulting composites are, in principle, determined by the properties of the initial CdTe nanocrystals in solution. Therefore, this new synthetic route opens up an alternative method to produce highly fluorescent CdTe–polymer composites with predictable properties. Moreover, the fluorescent microbeads of nanocrystal–polymer composite could find application in biological labeling.[8b] Further attempts are underway to produce micrometer-sized CdTe–PS beads by swelling crosslinked PS beads in a solvent mixture containing OVDAC-coated CdTe and styrene, and followed by the polymerization of composite CdTe nanocrystals in the swollen PS beads.

Experimental

A series of aqueous colloidal CdTe solutions were prepared by adding freshly prepared NaHTe solution to 1.25×10^{-3} N N_2-saturated $CdCl_2$ solutions at pH 9.0 in the presence of 3-mercaptocarboxylic acid (MPA) as a stabilizing agent [5,19]. The molar ratio of Cd^{2+}/MPA/HTe^- was fixed at 1:2.4:0.5. The resulting mixture was then subjected to reflux that controlled the growth of the CdTe nanocrystals. Octadecyl-*p*-vinylbenzyldimethylammonium chloride (OVDAC) was synthesized according to the procedure reported by Aoyagi et al. [23] and dissolved in styrene at a concentration of 2 mg mL^{-1}. 10 mL of OVDAC styrene solution was added to 20 mL of CdTe aqueous solution under vigorous stirring. The styrene phase was then separated and polymerized in a glass tube in an oil bath at 72~74 °C for 30 h using 0.2 wt.-% azobisisobutyronitrile (AIBN) as initiator. Transparent CdTe–polystyrene composites resulted. For more quantitative syntheses, chloroform was used instead of styrene. Powders of the OVDAC-coated CdTe was obtained after evaporation of chloroform and a drying process. Then the composite nanocrystals were redispersed quantitatively (from 0.1 wt.-% to 10 wt.-%) in styrene, which was followed by free-radical polymerization initiated by 0.2 wt.-% AIBN in an oil bath. CdTe–polystyrene/poly(methyl methacrylate) (PS/PMMA) composites were obtained in a similar way by dispersing CdTe–OVDAC in the mixture of methyl methacrylate and styrene with 10:1 volume ratio. The concentration of AIBN is 0.1 wt.-% in the following polymerization which was realized by a programmed heating process from 50 to 80 °C.

The relative PL quantum yields of all CdTe samples were estimated using Rohodamine 6G as PL reference [5,19]. For the measurement of PL quantum yield of CdTe in PS composites, composite plates were fabricated using a planar chamber as the polymerizing mode. The concentration of the inorganic nanocrystals in the polymer composites was characterized by thermogravimetric analysis (TGA), which was performed on a Mettler Netzsch STA 449C thermoanalysis instrument (Analyses were carried out under N_2 flow in the range of 30–800 °C with heating rate of 20.0 °C min^{-1}). For the CdTe–PS composite samples containing 10 wt.-% CdTe–OVDAC composites, the concentration of inorganic CdTe was around 3 wt.-%. This value was used to estimate the CdTe concentrations in other polymer composites by normalizing the absorption spectra of CdTe–OVDAC in corresponding monomer solutions. UV-vis transmission spectra were recorded by using a Shimadzu 3100 UV-vis near-infrared (NIR) spectrophotometer. Fluorescence experiments were performed with the help of a Shimadzu RF-5301 PC spectrofluorimeter. Transmission electron microgroscopy (TEM) images obtained on ultrathin sections of CdTe–PS composites were recorded by a JEOL-2010 electron microscope operating at 200 kV.

Received: October 11, 2002
Final version: January 31, 2003

[1] V. I. Klimov, A. A. Mikhailovsky, S. Xu, A. Malko, J. A. Hollingsworth, C. A. Leatherdale, H.-J. Eisler, M. G. Bawendi, *Science* **2000**, *290*, 314.
[2] K. Jacobs, D. Zaziski, E. C. Scher, A. B. Herhold, A. P. Alivisatos, *Science* **2001**, *293*, 1803.
[3] a) A. P. Alivisatos, *Science* **1996**, *271*, 933. b) Z. Tang, N. A. Kotov, M. Giersig, *Science* **2002**, *297*, 237. c) M. Nirmal, L. Brus, *Acc. Chem. Res.* **1999**, *32*, 407.
[4] L. Qu, Z. A. Peng, X. Peng, *Nano Lett.* **2001**, *1*, 333.
[5] M. Gao, S. Kirstein, H. Möhwald, A. L. Rogach, A. Kornowski, A. Eychmüller, H. Weller, *J. Phys. Chem. B* **1998**, *102*, 8360.
[6] a) V. L. Colvin, M. C. Schlamp, A. P. Alivisatos, *Nature* **1994**, *370*, 354. b) A. A. Mamedov, A. Belov, M. Giersig, N. N. Mamedov, N. A. Kotov, *J. Am. Chem. Soc.* **2001**, *123*, 7738.
[7] V. C. Sundar, H. Eisler, M. G. Bawendi, *Adv. Mater.* **2002**, *14*, 739.
[8] a) M. Bruchez, M. Moronne, P. Gin, S. Weiss, A. P. Alivisatos, *Science* **1998**, *281*, 2013. b) M. Han, X. Gao, J. Z. Su, S. Nie, *Nat. Biotechnol.* **2001**, *19*, 631. c) H. Mattoussi, J. M. Mauro, E. R. Goldman, G. P. Anderson, V. C. Sundar, F. V. Mikulec, M. G. Bawendi, *J. Am. Chem. Soc.* **2000**, *122*, 12 142.
[9] a) Y. W. Cao, U. Banin, *J. Am. Chem. Soc.* **2000**, *122*, 9692. b) D. Gerion, F. Pinaud, S. C. Williams, W. J. Parak, D. Zanchet, S. Weiss, A. P. Alivisatos, *J. Phys. Chem. B* **2001**, *105*, 8861. c) A. L. Rogach, D. Nagesha, J. W. Ostrander, M. Giersig, N. A. Kotov, *Chem. Mater.* **2000**, *12*, 2676. d) Y. A. Wang, J. J. Li, H. Chen, X. Peng, *J. Am. Chem. Soc.* **2002**, *124*, 2293. e) N. Gaponik, I. L. Radtchenko, B. Sukhorukov, H. Weller, A. L. Rogach, *Adv. Mater.* **2002**, *14*, 879.
[10] J. Lee, V. C. Sundar, J. R. Heine, M. G. Bawendi, K. F. Jensen, *Adv. Mater.* **2000**, *12*, 1102.
[11] N. Gaponik, D. V. Talapin, A. L. Rogach, A. Eychmüller, H. Weller, *Nano. Lett.* **2002**, *2*, 803.
[12] L. Erskine, T. Emrick, A. P. Alivisatos, J. M. J. Fréchet, *Polym. Prepr.* **2000**, *41*, 593.
[13] M. Gao, J. Sun, E. Dulkeith, N. Gaponik, U. Lemmer, J. Feldmann, *Langmuir* **2002**, *18*, 4098.
[14] M. Gao, Y. Yang, B. Yang, F. Bian, J. Sheng, *Chem. Commun.* **1994**, 2779.
[15] a) D. E. Fogg, L. H. Radzilowski, R. Blanski, R. R. Schrock, E. L. Thomas, *Macromolecules* **1997**, *30*, 417. b) H. Skaff, M. F. Ilker, E. B. Coughlin, T. Emrick, *J. Am. Chem. Soc.* **2002**, *124*, 5729.
[16] N. Gaponik, D. V. Talapin, A. L. Rogach, K. Hoppe, E. V. Shevchenko, A. Komowski, A. Eychmüller, H. Weller, *J. Phys. Chem. B* **2002**, *106*, 7177.
[17] a) Y. Tian, J. H. Fendler, *Chem. Mater.* **1996**, *8*, 969. b) D. G. Kurth, P. Lehmann, C. Lesser, *Chem. Commun.* **2000**, 949.
[18] T. Hirai, T. Watanabe, I. Komasawa, *J. Phys. Chem. B* **2000**, *104*, 8962.
[19] H. Zhang, Z. Zhou, B. Yang, M. Gao, *J. Phys. Chem. B* **2003**, *107*, 8.
[20] D. V. Talapin, A. L. Rogach, E. V. Shevchenko, A. Komowski, M. Haase, H. Weller, *J. Am. Chem. Soc.* **2002**, *124*, 5782.
[21] a) J. R. Lakowiez, I. Gryczynski, G. Piszezek, C. J. Murphy, *J. Phys. Chem. B* **2002**, *106*, 5363. b) N. O. Dantas, F. Qu, R. S. Silva, *J. Phys. Chem. B* **2002**, *106*, 7453.
[22] X. A. Fu, S. Qutubuddin, *Langmuir* **2002**, *18*, 5058.
[23] T. Aoyagi, O. Terashima, N. Suzuki, K. Matsui, Y. Nagase, *J. Controlled Release* **1990**, *13*, 63.

Templated Surface Sol–Gel Synthesis of SiO_2 Nanotubes and SiO_2-Insulated Metal Nanowires**

By *Nina I. Kovtyukhova*,* *Thomas E. Mallouk*, and *Theresa S. Mayer*

In the past few years there has been a dramatic increase in research activity on high aspect ratio inorganic nanoparticles. This work has been stimulated by the availability of new techniques for making nanotubes, wires, scrolls, and ribbons from various materials, and by interest in the new physical proper-

[*] Dr. N. I. Kovtyukhova,[+] Prof. T. E. Mallouk
Department of Chemistry, 152 Davey Laboratory
The Pennsylvania State University
University Park, PA 16802 (USA)
E-mail: nina@chem.psu.edu
Prof. T. S. Mayer
Department of Electrical Engineering
The Pennsylvania State University
University Park, PA 16802 (USA)
[+] Second address: Institute of Surface Chemistry, N.A.S.U., 17, General Naumov Str., 03680 Kyiv, Ukraine.

[**] We thank Dr. T. N. Jackson, L. Jia, and C.-C. S. Kuo for their help in conducting electrical measurements. This work has been supported by the DARPA Moletronics Program and the Office of Naval Research.

  DOI: 10.1002/adma.200304701

ties of these unique forms of matter. Research in this field is also driven by the real practical potential of using nanowires and nanotubes as components of field emitter displays, magnetic media, sensors, resonators, solar cells, and electronic circuits.

The chemical assembly of nanowires is now considered a potentially viable alternative to the conventional lithographic fabrication of nanoscale circuits, which is increasingly approaching physical and economic limits. Most assembly approaches to electronic circuits target defect-tolerant architectures in which cross-point arrays of nanowires and/or nanotubes connect device elements. The possibility of fabricating transistors, diodes, and memory elements from individual crossed semiconductor nanowires[1] and carbon nanotubes[2,3] has now been convincingly demonstrated. These arrays can be further integrated into patterns in order to make larger scale logic and memory circuits.[4–6] While most of this research has involved semiconductor nanowires and carbon nanotubes, noble metal nanowires are also of interest for circuit assembly.[7–9] Highly conductive metals offer some special advantages, particularly as low-resistance interconnects in high-speed circuits. A further reduction in RC and LC (resistance–capacitance and inductance–capacitance) time constants for nanoscale circuits can be expected if low dielectric constant materials can be introduced as insulating spacers between metallic nanowires.[10]

A wide variety of elemental (metal, carbon, silicon, germanium) and compound (metal chalcogenides, metal oxide, III–V compound) nanowires and nanotubes are now available with metallic, semiconducting, and insulating electronic properties. In general, these high aspect ratio nanoparticles are prepared either from the vapor or solution phase, by one-dimensional growth from a seed or by growth on top or inside a template. Both methods now allow relatively simple preparation of composite concentric structures from components with different electronic properties.[7,11–16] Some of the particular advantages of the ambient temperature pore replication method are relatively easy access to bulk quantities of tubular structures,[7,11,17,18] the incorporation of inorganic and/or organic mono- and multilayer stripes and/or shells,[7,8] and the preparation of concentric nanowire structures with open tips that are accessible to further functionalization.[7,13]

Nanotubes of different compositions have been grown as thin films on the walls of cylindrical pores of membranes using preparative techniques developed for planar thin films. Conventional sol–gel methods, which involve immersing an anodic aluminum oxide membrane in a precursor sol followed by gelation inside the pores, have been used to prepare free-standing TiO_2, ZnO, WO_3, MnO_2, Co_3O_4, and SiO_2[17,19] nanotubes. In this method, internal nanotube diameter can be adjusted by varying concentration and viscosity of the initial sol as well as the immersion time. However, precise control over their thickness and morphology, especially for those tubes that are only a few nanometers thick, has not been demonstrated yet.

More reliable control over the quality of planar thin films has been realized in layer-by-layer deposition methods, in which i) preformed colloidal particles[20] or ii) molecular precursors[21–23] are successively adsorbed as a layer at a time onto the growing surface. Recently we demonstrated applicability of the first layer-by-layer technique to membrane substrates by preparing uniform and smooth free-standing semiconductor/polymer nanotubes and coated metal wires.[7]

The second, "surface sol–gel" (SSG) method, involves repeats of two-step deposition cycles, in which the adsorption of a molecular precursor and the hydrolysis (in the case of oxide film growth) steps are separated by a post-adsorption wash. The washing step desorbs weakly bound molecules that form additional layers.[22] Ideally, the SSG technique can limit each adsorption cycle to a single monolayer. However, in practice, thicker layers have been found for planar oxide SSG films.[22,23] Nevertheless, SSG allows very fine control over film thickness because a nanometer or sub-nanometer thick layer is grown in each two-step adsorption/hydrolysis cycle.

Here we report synthesis of silica nanotubes in anodic aluminum oxide membranes (AAO) using the SSG technique. To attempt to understand the dynamics of the tube growth, the process has been monitored by transmission electron microscopy (TEM) and SiO_2 mass uptake measurements. While still in the membrane, the SiO_2-coated pores can be electrochemically filled with metal and then released by etching in acid to give free-standing insulated wires. We have electrically characterized these insulated wires, and report here that the SSG method gives a very high-quality dielectric oxide.

Silicon oxide nanotubes were grown inside AAO membranes as shown schematically in Figure 1, route 1. In the first step, $SiCl_4$ molecules are adsorbed on the hydrated surface of

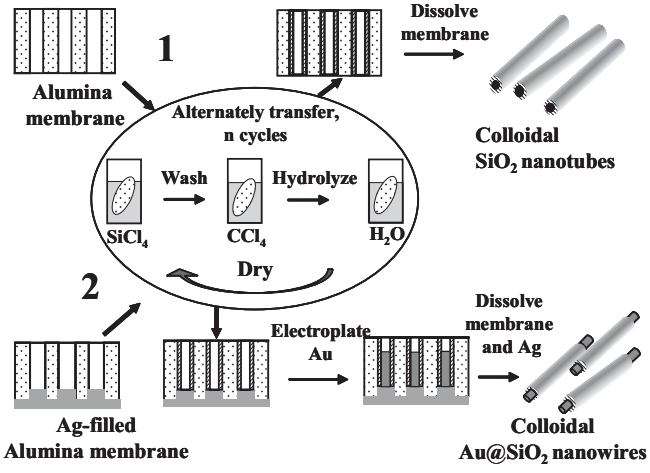

Fig. 1. Scheme showing the SSG synthesis of SiO_2 nanotubes (route 1) and SiO_2-coated nanowires (route 2).

the alumina membrane. Subsequent washing with CCl_4 removes the unbound adsorbate molecules from the pores. In the second step, the adsorbed $SiCl_4$ is hydrolyzed to give SiO_2. Free-standing nanotubes were obtained by etching the alumina membranes in 50 % H_2SO_4. Energy-dispersive X-ray (EDX) analysis of the product showed Si and O, with no detectable ($\leq$0.5 %) Cl or Al. Hence the conversion of $SiCl_4$ to

ADVANCED MATERIALS

silica is complete, and no alumosilicate phase is present. This allows us to describe the chemical composition of the oxide as $(SiO_2)_x(SiOH)_y$.

TEM images (Fig. 2a,b) show robust SiO_2 nanotubes with smooth and uniform walls. Their shape clearly replicates the pore structure of AAO, including branches. Tubes 20–30 μm long can be found in optical micrographs (not shown), implying the growth of continuous tubules along the pore length. Figure 2a illustrates the remarkably high flexibility of these long silica nanotubes. A 100 nm diameter tube grown in five deposition cycles does not break even when bent at right angles. The external diameter of the tubes is determined by the pore diameter, and their internal diameter is adjustable by varying the number deposition cycles and/or the concentration of $SiCl_4$. Nanotubes with external diameters ranging from 40 to 300 nm, and with wall thicknesses from 2 to 30 nm, were prepared. The dependence of the nanotube wall thickness (which was estimated from TEM images of metal-filled nanotubes (Fig. 2c,d)) on the number of the deposition cycles is shown in Figure 3a, trace 1. The graph is not linear: the amount of SiO_2 deposited per cycle increases gradually as the tubes are grown. For example, under the conditions shown in Figure 3a, trace 1, the thickness change per cycle increases from 8.7 Å in the 4th–10th cycles to 15.3 Å in the 10th–20th cycles. Both values exceed the film thickness increase (~3 Å) expected if only one Si–O–H monolayer is added per cycle. The shape of this film thickness graph closely resembles that of the mass uptake of SiO_2 (Fig. 3a, trace 2). This correlation allows one to follow the process of nanotube growth by simply weighing the dry membrane after each SSG cycle.

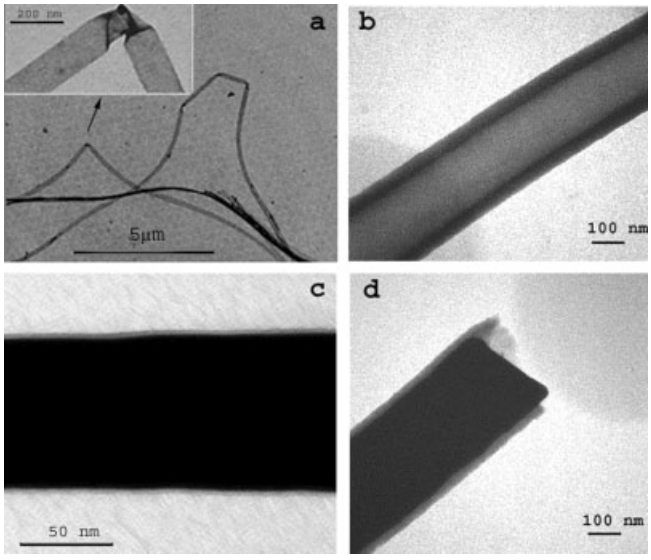

Fig. 2. TEM images of a,b) SiO_2 nanotubes, and c,d) Au wires grown inside the SiO_2 nanotubes. a,c) Five deposition cycles in 90 ± 20 nm diameter pores. b,d) 20 deposition cycles in 280 ± 20 nm diameter pores.

The film growth at different $SiCl_4$ concentrations is shown in Figure 3b. At any $SiCl_4$ concentration, a steep rise is observed in the first deposition cycle. After this, the film growth slows down significantly but the amount of SiO_2 deposited per cycle gradually increases. Ferguson and co-workers[24] attributed upward curvature in layer-by-layer growth of clay films to island nucleation and growth; however, this model is not consistent with the smooth morphology of SSG silica films seen in the TEM images.

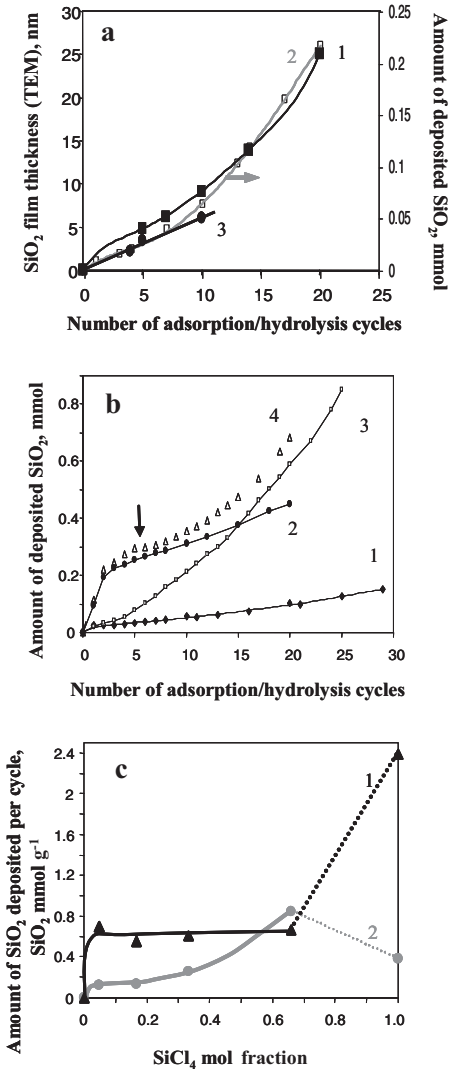

Fig. 3. a) Plots of SiO_2 wall thickness (1,3) and amount of SiO_2 deposited (2) from a 67 mol-% solution of $SiCl_4$ versus the number of deposition cycles: pore diameter 280 ± 20 nm (1,2) and 90 ± 20 nm (3). b) Amount of SiO_2 deposited versus the number of deposition cycles for different concentrations of $SiCl_4$ in CCl_4: 1) 5 mol-%; 2) 100 mol-%; 3) 67 mol-%; 4) 100 mol-% $SiCl_4$ was used in the first five cycles and 67 mol-% $SiCl_4$ was used in the next 15 cycles; arrow shows the point where the concentration was changed. Pore diameter 280 ± 20 nm. c) Amount of SiO_2 deposited per cycle on alumina (1) and silica-covered (2) membrane surface versus $SiCl_4$ mole fraction. Pore diameter 280 ± 20 nm, bare membrane weight 0.033 g ± 2 %.

Another possibility is that the upward curvature arises from occlusion of water in the growing film. Water is always present as a surface layer on hydrophilic surfaces under ambient conditions. The extent to which this surface-bound water will result in multilayer deposition depends on the amount of water present, the extent to which H_2O and CCl_4 molecules compete for interaction with $SiCl_4$, and the permeability of the deposited $[SiOCl_x(OH)_y]_n$ film to water, $SiCl_4$, and CCl_4.

The coexistence of these three factors may cause the complex character of graphs shown in Figures 3b and 3c. The fact that multiple layers of SiO_2 are grown in each cycle indicates that at high concentration, a multilayer of $SiCl_4$ molecules is present in the adsorption layer. In the subsequent washing step with CCl_4, all unreacted (unbound) $SiCl_4$ is removed. The following SSG step (immersion in water) completes hydrolysis of any remaining Si–Cl bonds and restores the water surface layer.

We suggest that the amount of SiO_2 deposited in each SSG cycle is mainly determined by the amount of $SiCl_4$ adsorbed in the first step rather than by the hydrolysis step. In this case, a plot of SiO_2 amount deposited per cycle (ΔSiO_2) versus $SiCl_4$ mole fraction can be considered as a qualitative analogue of a $SiCl_4$ adsorption isotherm. Figure 3c traces 1,2 shows two such plots taken 1) for the first deposition cycle and 2) as an average for the range of 5th–10th cycles, in which SiO_2 deposition is linear for all concentrations. The first isotherm (Fig. 3c trace 1) characterizes $SiCl_4$ adsorption on the alumina surface while the second one (Fig. 3c trace 2) is related to silica surface adsorption since, according to the TEM data, the pore walls are completely covered with SSG film after five cycles. The low concentration region of both plots is concave to the concentration axis, which is characteristic of strong interaction between surface and adsorbate,[25] and is consistent with the chemical reaction of $SiCl_4$ with H_2O covered alumina and silica surfaces. It is evident from the low concentration region of the plots that the $SiCl_4$ interaction with the alumina/H_2O surface is stronger. Further flow of the adsorption isotherms for alumina and silica surfaces is different. On the silica/H_2O surface, the amount of SiO_2 deposited, as expected, increases gradually with the $SiCl_4$ mole fraction. However on the alumina surface, the plot has a long plateau parallel to the concentration axis. We suggest that in the $SiCl_4$ mole fraction range of 0.05–0.67, fast formation of the $[SiOCl_x(OH)_y]_n$ layer at the alumina/H_2O//($SiCl_4$+CCl_4) interface occurs, and this layer is dense enough to block further penetration of $SiCl_4$ through the film. An increase in adsorption on the alumina surface is observed when the $SiCl_4$ mole fraction equals 1. Apparently, in the absence of CCl_4 the hydrolysis reaction can continue until all water in the surface layer is consumed and replaced by the $[SiOCl_x(OH)_y]_n$ layer. Hence the amount of water available for hydrolysis of $SiCl_4$ determines its adsorption value. The fact that film growth is faster on the alumina pore walls (Fig. 3c, trace 1) than it is on several layers of the SSG film (Fig. 3c, trace 2) is consistent with the idea that the more polar alumina surface retains more water. Interestingly, in the plot of film grown on the silica/H_2O surface, a higher adsorption value is found at the $SiCl_4$ mole fraction of 0.67 than at that of 1 (Fig. 3c, trace 2).

Heat-treatment (100 °C, 3–13 h) of SiO_2-containing membranes dried at ambient temperature in Ar results in a weight loss of ~4 %, which can be ascribed to the removal of unbound water from the SiO_2 film. This indicates that the SiO_2 film is relatively porous, and the pore fraction is estimated to be ~0.09 taking the SiO_2 density at 2.17 g cm^{-3}.[26] This porosity is associated with relatively large pores and does not include micropores (if any) with radii approaching the thickness of an adsorbed water layer, because water in those pores can only be removed at higher temperatures. The porous structure of the SiO_2 film is consistent with the idea of occluded water assisting in multilayer film growth and is likely to be responsible for the gradual increase in the amount of SiO_2 deposited per cycle (Fig. 3a,b) rather than narrowing the pores during the SSG procedure. The tube growth inside the 90 nm wide pores is not found to be faster than that inside the 280 nm wide pores (Fig. 3a, traces 1,3).

The same percent weight loss is observed for initial $SiCl_4$ concentrations of 5 mol-%, 16 mol-%, 33 mol-%, and 100 mol-%, while for 67 mol-% $SiCl_4$ solution, the weight loss is 5.6 % after the 10th and 10 % after the 20th deposition cycle. Accordingly, the estimated porosity is 0.126 for the SiO_2 film deposited in ten cycles and it increases to 0.225 during the next ten cycles. The porosity of the SiO_2 film measured under different growth conditions is consistent with the data shown in Figure 3. In a 100 % $SiCl_4$ solution the layer growth is actually slower than it is at 67 mol-% $SiCl_4$ (Fig. 3b, traces 2,3). The 100 mol-% solution gives lower film porosity (0.09 after five deposition cycles), but upward curvature in film growth is found (Fig. 3b, trace 4) if the concentration is lowered to 67 mol-%, which provides higher porosity (0.144 after 15 cycles). These facts suggest that, at relatively low CCl_4 concentration, thicker and more poorly ordered $[SiOCl_x(OH)_y]_n$ layers, which may occlude both H_2O and CCl_4 molecules, are formed at the adsorption step of SSG cycles. Thus by an appropriate selection of synthesis conditions, one can control not only the thickness of nanotube walls, but also their porosity.

SiO_2-insulated metal nanowires were prepared as shown schematically in Figure 1, route 2, using a conventional electrochemical plating technique.[27] Typical TEM images (Fig. 2c,d) show the gold wires inside uniformly thick and smooth silica tubes. The tube walls remain defect-free and no metal penetration of the walls is seen. The top ends of the wires are typically flat or convex, unlike nanowires grown in unmodified alumina membranes, which have cup-shaped ends. This cup-like shape has been explained as a consequence of the high surface tension of the alumina pore walls.[7] The interaction of gold with the less polar silica pores is apparently weaker. The coulombic efficiency for plating Au and Ni wires is about 1.2 times higher (judging from wire lengths) in silica-modified pores than it is in unmodified anodic alumina.

When the silica-coated nanowires are released from the membrane, both ends are open, because the tube shells break near the ends of the metal wire (Fig. 2d). This allows one to make electrical contact by evaporating metal onto the wire ends.

The current–voltage (I–V) characteristics of SSG SiO_2 films of different thicknesses (measured in Au@SiO_2/Au configuration) are shown in Figure 4 (top). The curves show typical insulating behavior with breakdown voltages that increase

ADVANCED MATERIALS

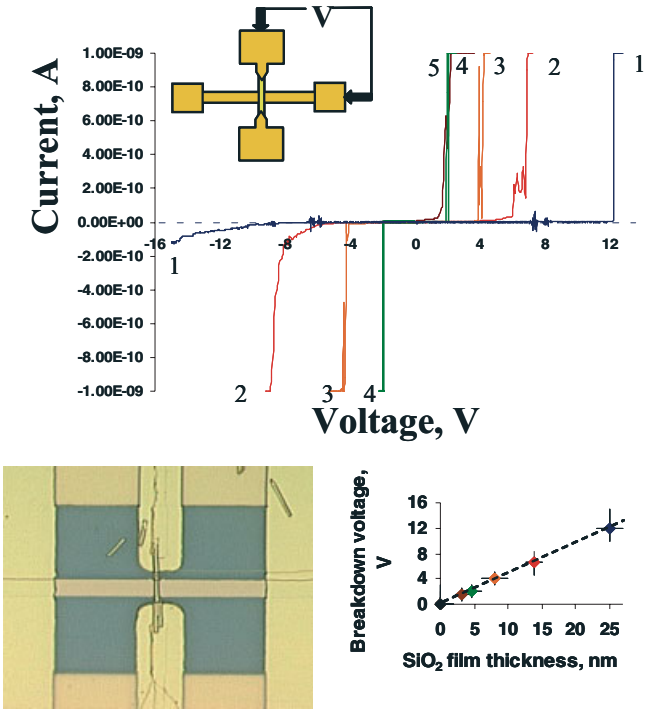

Fig. 4. Top: *I–V* characteristics of SiO_2-coated gold nanowires with different thickness of SiO_2 [nm]: 1) 25, 2) 14, 3) 8, 4) 4.5, 5) 3.5. A scheme of a test structure for measuring the electrical properties is shown in the inset. Bottom: Optical micrograph of a test structure for measuring the electrical properties of SiO_2-coated gold nanowires (left). A plot of the breakdown voltage versus thickness (right).

linearly with film thickness (Fig. 4, bottom). The hard breakdown field is estimated at 4.8 MV cm^{-1}, which is only slightly less than the breakdown fields (10–15 MV cm^{-1}) of the SiO_2 dielectric used in complementary metal oxide semiconductor (CMOS) integrated-circuit technology.

Because the SiO_2 tubes are porous, their dielectric constant is expected to be lower than that of dense silica ($\varepsilon = 3.8$[10]). Porous silica is a promising dielectric material for nanoelectronics applications because of its relatively low dielectric constant.[28] Theoretical calculations predict a dielectric constant of 1.8–2.8 for a volume pore fraction of 0.4, and an almost linear decrease in ε with increasing porosity. In our experiments, it was difficult to measure the dielectric constant of the SiO_2 films precisely because of the uncertainty in the contact area in the Au@SiO_2/Au configuration. Nevertheless it is interesting to note that the synthesis offers some control over porosity, and that this will probably be reflected in the dielectric constant of the films.

In conclusion, the surface sol–gel method is a simple way to prepare robust and flexible silica nanotubes and nanotube-encapsulated metal nanowires. The thickness and porosity of the tubes can be precisely controlled by varying the composition of the precursor solution and the number of adsorption/hydrolysis cycles. The thickness of the SiO_2 layer deposited in each cycle, which always exceeds that of a monomolecular layer, can be explained assuming occlusion of water present as a surface layer. Free-standing SiO_2 nanotubes with 2–30 nm thick walls, which are smooth and uniform along their length, were grown and characterized. The hard breakdown field obtained for insulating SiO_2 nanotube coating on gold nanowires is only slightly lower than that of SiO_2 dielectric used in CMOS integrated circuits, and this is a surprising result given the fact that a wet chemical deposition method was used.

The SSG thin film deposition technique is well developed for other classes of materials, including metal oxides, chalcogenides, and phosphates. When performed in porous templates, as we have demonstrated here for SiO_2, the SSG method should offer a route to concentric multicomponent structures with well-controlled layer thickness and, presumably, tunable electrical and optical properties. The good control in film thickness that is obtained by SSG suggests that it should also be possible to precisely adjust the internal diameter of the AAO pores, and hence the diameter of nanowire replicas.

Experimental

SiO_2 Nanotubes: These were prepared as follows. Commercial (Whatman Anodisc 25) and homemade membranes 60–35 μm thick with a pore diameter of 280 ± 20 nm, 90 ± 20 nm, and 55 ± 15 nm were used. A membrane was immersed in a $SiCl_4$ (Acros) solution in CCl_4 (5–100 mol-%) for 2 min and quickly washed with CCl_4 to remove the reagent from the faces. The membrane was then placed in a beaker with a fresh portion of CCl_4 for 15–30 min to remove unbound $SiCl_4$ from the pores. Finally, the membrane was soaked in CCl_4/MeOH 1:1 (2 min) and EtOH (5 min) to displace CCl_4, and dried in an Ar stream. Then the membrane was immersed in deionized water for 5 min, washed in a beaker with MeOH (2 min), and dried in an Ar stream. To make sure that all the $SiCl_4$ was washed away from the pores, we conducted several control experiments with washing performed under vacuum in a suction filtering unit. Both washing procedures resulted in the same amount of deposited SiO_2. Drying the membrane before each adsorption and hydrolysis step removes the residual reagents (if any) and solvents from the pores and provides quick convective transport of the reagents in the next step. Longer times for each step did not have noticeable effects on the amount of SiO_2 deposited. This implies that the shape of graphs shown in Figure 3c cannot be attributed to a simple kinetic effect.

Insulated Metal Nanowires: These were prepared as follows. An alumina membrane with a thin Ag film evaporated on its branched side was used as a cathode in an electrochemical cell equipped with a Pt wire anode and a saturated calomel electrode (SCE) reference electrode. First, 15–20 μm long Ag wires were grown inside the membrane to fill the branched part of the pores. SiO_2 tubes were then grown on the exposed pore walls, and 5–8 μm long Au nanowires were electroplated inside the tubes in potentiostatic mode at –0.9 V. The Ag backing and the alumina membrane were dissolved in 50 % HNO_3 and 50 % H_2SO_4, respectively.

Electrical Measurements: SiO_2-coated Au nanowires (Au@SiO_2) were aligned between two metal pads on a lithographically patterned Si substrate using an electrofluidic method described elsewhere [29]. Electrical contacts were fabricated by evaporating 200 nm thick Au pads on top of the wire ends and 50 nm thick Au lines on top of the SiO_2 coating (Fig. 4, bottom left). In some experiments, electrical contact to the SiO_2 coating was made by electrofluidically positioning the nanowires over the Au lines (inset in Fig. 4, top). *I–V* characteristics were recorded with Precision Semiconductor Parameter Analyzer Hewlett Packard 4156B.

Received: November 30, 2002
Final version: January 23, 2003

[1] Y. Huang, X. Duan, Y. Cui, L. Lauhon, K. Kim, C. M. Lieber, *Science* **2001**, *294*, 1313.
[2] T. Rueckes, K. Kim, E. Joselevich, G. Tseng, C.-L. Cheung, C. M. Lieber, *Science* **2000**, *289*, 94.
[3] A. Bachtold,P. Hadley, T. Nakanishi, C. Dekker, *Science* **2001**, *294*, 1317.

[4] G. Tseng, J. Ellenbogen, *Science* **2001**, *294*, 1293.
[5] S. C. Goldstein, M. Budiu, in *Proc. 28th Annu. Int. Symp. Computer Architecture*, *2001*, ACM Press, New York **2001**, p. 178.
[6] N. I. Kovtyukhova, T. E. Mallouk, *Chem. Eur. J.* **2002**, *8*, 4354.
[7] a) N. I. Kovtyukhova, B. R. Martin, J. K. N. Mbindyo, P. A. Smith, B. Razavi, T. S. Mayer, T. E. Mallouk, *J. Phys. Chem. B* **2001**, *105*, 8762. b) N. I. Kovtyukhova, B. R. Martin, J. K. N. Mbindyo, T. E. Mallouk, M. Cabassi, T. S. Mayer, *Mater. Sci. Eng., C* **2002**, *19*, 255.
[8] J. K. N. Mbindyo, T. E. Mallouk, I. Kratochvilova, B. Razavi, T. S. Mayer, T. N. Jackson, J. B. Mattzela, *J. Am. Chem. Soc.* **2002**, *124*, 4020.
[9] D. J. Pena, J. K. N. Mbindyo, A. J. Carado, T. E. Mallouk, C. D. Keating, B. Razavi, T. S. Mayer, *J. Phys. Chem. B* **2002**, *106*, 7458.
[10] *Handbook of Low and High Dielectric Constant Materials and Their Applications, V1* (Ed: H. S. Nalwa), Academic Press, San Diego, CA **1999**.
[11] V. M. Cepak, J. C. Hulteen, G. Che, K. B. Jirage, B. B. Lakshmi, E. R. Fisher, C. R. Martin, *Chem. Mater.* **1997**, *9*, 1065.
[12] L. J. Lauhon, M. S. Gudiksen, D. Wang, C. M. Lieber, *Nature* **2002**, *420*, 57.
[13] J. S. Yu, J. Y. Kim, S. Lee, J. K. N. Mbindyo, B. R. Martin, T. E. Mallouk, *Chem. Commun.* **2000**, 2445.
[14] a) G. Schnur, R. Price, P. Schoen, P. Yager, *Thin Solid Films* **1987**, *152*, 181. b) E. Braun, Y. Eichen, U. Sivan, G. Ben-Yoseph, *Nature* **1998**, *391*, 775. c) R. Yu, L. Chen, Q. Liu, J. Lin, K. Tan, S. Ng, H. Chan, G. Xu, T. Hor, *Chem. Mater.* **1998**, 10, 718. d) Q. Fu, C. Lu, J. Liu, *Nano Lett.* **2002**, *2*, 329.
[15] a) S. O. Obare, N. R. Jana, C. J. Murphy, *Nano Lett.* **2001**, *1*, 601. b) Y. Yin, Y. Lu, Y. Sun, Y. Xia, *Nano Lett.* **2002**, *2*, 427.
[16] X. Shi, S. Han, R. J. Sanedrin, C. Galvez, D. J. Ho, B. Hernandez, F. Zhou, M. Selke, *Nano Lett.* **2002**, *2*, 289.
[17] a) D. T. Mitchell, S. B. Lee, L. Trofin, N. Li, T. K. Nevanen, H. Soderlund, C. R. Martin, *J. Am. Chem. Soc.* **2002**, *124*, 11 864. b) B. B. Lakshmi, P. K. Dorhout, C. R. Martin, *Chem. Mater.* **1997**, *9*, 857. c) B. B. Lakshmi, C. J. Patrissi, C. R. Martin, *Chem. Mater.* **1997**, *9*, 2544.
[18] M. Wirtz, M. Parker, Y. Kobayashi, C. Martin, *Chem. Eur. J.* **2002**, *8*, 3573.
[19] M. Zhang, Y. Bando, K. Wada, *J. Mater. Res.* **2000**, *15*, 187.
[20] a) R. K Iler, *J. Colloid Interface Sci.* **1966**, *21*, 569. b) V. L. Colvin, A. N. Golstein, A. P. Alivisatos, *J. Am. Chem. Soc.* **1992**, *114*, 5221. c) J. Fendler, *Chem. Mater.* **1996**, *8*, 1616. d) T. E. Mallouk, H.-N. Kim, P. J. Ollivier, S. W. Keller, in *Comprehensive Supramolecular Chemistry*, Vol. 7 (Eds: G. Alberti, T. Bein), Elsevier Science, Oxford **1996**, p. 189.
[21] Y. F. Nicolau, J. C. Menard, *J. Cryst. Growth* **1988**, *92*, 128.
[22] a) I. Ichinose, H. Senzu, T. Kunitake, *Chem. Mater.* **1997**, *9*, 1296. b) M. Fang, C. H. Kim, B. R. Martin, T. E. Mallouk, *J. Nanoparticle Res.* **1999**, *1*, 43.
[23] N. I. Kovtyukhova, E. V. Buzaneva, C. C. Waraksa, B. Martin, T. E. Mallouk, *Chem. Mater.* **2000**, *12*, 383.
[24] E. R. Kleinfeld, G. S. Ferguson, *Chem. Mater.* **1996**, *8*, 1575.
[25] *Adsorption from Solution at the Solid/Liquid Interface* (Eds: G. D. Parfitt, C. H. Rochester), Academic Press, London **1983**.
[26] *Handbook of Chemistry and Physics*, 68th ed. (Ed: R. C. Weast), CRC Press, Boca Raton, FL **1987–88**.
[27] a) D. Al-Mawlawi, C. Z. Liu, M. Moskovits, *J. Mater. Res.* **1994**, *9*, 1014. b) M. Nishizava, V. P. Menon, C. R. Martin, *Science* **1995**, *268*, 700.
[28] C. Jin, J. D. Luttmer, D. M. Smith, T. A. Ramos, *MRS Bull.* **1997**, *22(10)*, 39.
[29] P. A. Smith, C. D. Nordquist, T. N. Jackson, T. S. Mayer, B. Martin, J. Mbindyo, T. E. Mallouk, *Appl. Phys. Lett.* **2000**, *77*, 1399.

A Novel Photochromic Film by Oxidation Polymerization of a Bisbenzothienylethene with Phenol Groups**

By *Kingo Uchida*,* *Atsushi Takata*, *Masaaki Saito*, *Akinori Murakami*, *Shinichiro Nakamura*, and *Masahiro Irie*

Photochromic molecules attract much attention from both fundamental as well as practical points of view because of their potential for applications in optical devices such as optical memories and switches.[1] Among various photochromic compounds, diarylethenes are regarded as the best candidates, because of the thermal stability of both isomers and their fatigue resistance.[2] For applications, it is essential to fabricate thin photochromic films. The most convenient method for preparing photochromic films is to disperse photochromic molecules into polymer films.[3] Although higher dye concentrations are strongly desired in order to enhance photochromic efficiency, the preparation of thin films containing high concentrations of dyes is not easy, because, after long term storage, segregation takes place to some extent. Crystalline photochromism has also been extensively studied for solid photochromic materials.[4] However, it is difficult to fabricate crystalline thin films.

Here, we present a novel method for preparing diarylethene photochromic thin films, in which the diarylethene molecules were densely packed and the photochromism could be non-destructively monitored by infrared absorption measurements.[5] In the films, diarylethene molecules were fixed in a photoreactive antiparallel (a-p) conformation[2a] by crosslinking.[6] Therefore, the films were expected to have high photosensitivity.

1,2-Bis[2-methyl-6-(*o*-hydroxyphenyl)-1-benzothiophen-3-yl]hexafluorocyclopentene (**1a**) was synthesized according to the literature procedure,[7,8] and oxidation polymerization of the closed-ring isomer **1b** yielded thin photochromic films (see Scheme 1).

Figure 1 illustrates the absorption spectral changes of an ethyl acetate solution of **1a** (1.78×10^{-5} mol L^{-1}). Upon irradiation with UV light ($\lambda = 313$ nm), the solution turned to

[*] Prof. K. Uchida, A. Takata, M. Saito
Department of Materials Chemistry, Faculty of Science and Technology
Ryukoku University
Seta, Otsu 520-2194 (Japan)
E-mail: uchida@chem.ryukoku.ac.jp
A. Murakami, Dr. S. Nakamura
MCC-Group Science & Technology Research Center
Mitsubishi Chemical Corporation and ACT
Japan Science and Technology Corporation (JST)
1000 Kamoshida, Yokohama 227-8502 (Japan)
Prof. M. Irie
Department of Chemistry and Biochemistry
Graduate School of Engineering, Kyushu University
6-10-1 Hakozaki, Fukuoka 812-8581 (Japan)

[**] We thank Mr. Mitsuhiko Morimoto and Mr. Koshiro Yamakawa of Perkin Elmer Japan Co., Ltd. Osaka Branch Office for the use of Perkin Elmer Spectrum Spotlight 300. This work was supported by ACT of Japan Science and Technology Cooperation (JST), Sumitomo Foundation, and a Grant-in-Aid for Scientific Research (C) No. 12 640 567 from the Ministry of Education, Science, Sports, and Culture.

 DOI: 10.1002/adma.200304562